Physics-Informed Deep Learning for Musculoskeletal Modeling: Predicting Muscle Forces and Joint Kinematics From Surface EMG

Jie Zhang, *Member, IEEE*, Yihui Zhao, Fergus Shone, Zhenhong Li, *Member, IEEE*, Alejandro F. Frangi, *Fellow, IEEE*, Sheng Quan Xie, *Senior Member, IEEE*, and Zhi-Qiang Zhang, *Member, IEEE*

***Abstract*— Musculoskeletal models have been widely used for detailed biomechanical analysis to characterise various functional impairments given their ability to estimate movement variables (i.e., muscle forces and joint moments) which cannot be readily measured in *vivo*. Physics-based computational neuromusculoskeletal models can interpret the dynamic interaction between neural drive to muscles, muscle dynamics, body and joint kinematics and kinetics. Still, such set of solutions suffers from slowness, especially for the complex models, hindering the utility in real-time applications. In recent years, data-driven methods have emerged as a promising alternative due to the benefits in speedy and simple implementation, but they cannot reflect the underlying neuromechanical processes. This paper proposes a physics-informed deep learning framework for musculoskeletal modelling, where physics-based domain knowledge is brought into the data-driven model as soft constraints to penalise/regularise the data-driven model. We use the synchronous muscle forces and joint kinematics prediction from surface electromyogram (sEMG) as the exemplar to illustrate the proposed framework. Convolutional neural network (CNN) is employed as the deep neural network to implement the proposed framework. Simultaneously, the physics law between muscle forces and joint kinematics is used the soft constraint. Experimental validations on two groups of data, including one benchmark dataset and one self-collected dataset from six healthy subjects, are performed. The experimental results demonstrate the effectiveness and robustness of the proposed framework.**

***Index Terms*— Musculoskeletal modelling, deep neural network, physics-based domain knowledge, muscle forces and joint kinematics prediction.**

Manuscript received 9 May 2022; revised 10 November 2022; accepted 27 November 2022. Date of publication 5 December 2022; date of current version 1 February 2023. This work was supported in part by U.K. Engineering and Physical Sciences Research Council (EPSRC) under Grant EP/S019219/1 and Grant EP/V057782/1 and in part by the European Union (EU) Marie Curie Individual Fellowship under Grant 101023097. *(Corresponding authors: Zhi-Qiang Zhang; Alejandro F. Frangi.)*

This work involved human subjects or animals in its research. Approval of all ethical and experimental procedures and protocols was granted by the MaPS and Engineering Joint Faculty Research Ethics Committee of the University of Leeds under Application No. MEEC 18-002.

Jie Zhang, Yihui Zhao, Zhenhong Li, Sheng Quan Xie, and Zhi-Qiang Zhang are with the School of Electronic and Electrical Engineering, University of Leeds, LS2 9JT Leeds, U.K. (e-mail: eenjz@leeds.ac.uk; eenyzhao@leeds.ac.uk; z.h.li@leeds.ac.uk; s.q.xie@leeds.ac.uk; z.zhang3@leeds.ac.uk).

Fergus Shone is with the School of Computing, University of Leeds, LS2 9JT Leeds, U.K. (e-mail: mm16f2s@leeds.ac.uk).

Alejandro F. Frangi is with the School of Computing, University of Leeds, LS2 9JT Leeds, U.K., also with the Alan Turing Institute, NW1 2DB London, U.K., and also with the Department of Electrical Engineering, KU Leuven, 3000 Leuven, Belgium (e-mail: a.frangi@leeds.ac.uk).

Digital Object Identifier 10.1109/TNSRE.2022.3226860

I. Introduction

HUMAN movements encompass complex interactions of the neuromuscular system [1]. As a powerful computational simulation tool, musculoskeletal model can be applied for detailed biomechanical analysis to understand these interactions, which would be beneficial to various applications ranging from evaluating rehabilitation treatment [2], enhancing performance of athletes [3], [4], optimising robotic design for impaired individuals [5], to surgical planning and intervention [6].

Thus far, the majority of the musculoskeletal models are based on physics-based modelling technique to interpret transformation among neural excitation, muscle dynamics, and joint kinematics and kinetics [7], [8], [9]. Via employing experimental recordings, e.g., electromyograms (EMGs), foot-ground reaction forces (GRFs), and segmental body kinematics, these models can provide non-invasive estimation for physiological quantities, such as muscle forces and the joint moment [10]. However, these models often suffer from the redundancy issue since the countless number of potential neural solutions can be employed to execute a single movement. Thus, static optimisation is commonly applied to solve this redundancy problem, which involves the use of inverse dynamics to track external joint moments and/or joint kinematics and estimation of muscle forces to satisfy pre-selected objective criteria, such as minimisation of the muscle activation squared [11], [12]. An alternative approach is to use EMG-driven neuromusculoskeletal models, consisting of a neural-driven forward dynamics model and static optimisation element [13], [14]. EMG can be used to calibrate musculotendon parameters of the model to individual properties (i.e., tendon slack length and optimal fiber length, etc.), via the optimisation procedure to best match experimental and estimated joint moments. It also enhances the joint torque estimation with static optimisation by adjusting the experimental EMG signals and synthesising the muscle excitations [15]. Although EMG-driven models overcome the limitations of static optimisation and are readily

available in the past years, they are time-consuming with high running latency [16]. It thus limits the models' utility for real-time applications.

To address the time-consuming issues of physics-based musculoskeletal models, data-driven models have also been explored to establish relationships between movement variables and neuromuscular status, i.e., from EMGs to joint kinematics and muscle forces [17], [18], [19], [20]. A major advantage of these data-driven models over physics-based models is speed. Although training may be lengthy, as inference involves a relatively simple forward pass through the network, it is computationally inexpensive and thus very quick. For instance, Hu et al. [21] utilised the long short-term memory (LSTM) network to estimate grasping forces from high-density surface EMGs (sEMGs). Geng et al. [22] proposed a convolution with attention mechanism network (CNN-Attention) for continuous finger kinematics prediction from sEMGs. Rane et al. [23] employed a deep neural network to learn the feature mapping from movement space to muscle space, so musculoskeletal force could be predicted from kinematics. Similar ideas were also reported in [24], [25], [26], [27]. In addition to the muscle force or joint kinematics prediction separately, there are some works predicting the muscle forces and joint loading/movement simultaneously. For example, Burton et al. [28] implemented four machine/deep learning methods, including recurrent neural network (RNN), convolutional neural network (CNN), fully-connected neural network, and principal component regression, to predict trend and magnitude of the estimated joint contact and muscle forces. Johnson et al. [29] utilised CNN to predict ground reaction forces and moments outside the laboratory setting. However, all these models are established without explicit physics modelling of the underlying neuromechanical processes, and they are essentially "black-box" tools where all intermediate functional relationships cannot reflect the mechanisms underlying the observed variables [30], [31].

To address the drawbacks above of both physics-based and data-driven models, a physics-informed deep learning musculoskeletal model framework is proposed in this paper, which can seamlessly integrate the existing physics-based domain knowledge into the data-driven models. It will therefore overcome limitations associated with both types of musculoskeletal models while preserving their advantages. We use the synchronous muscle forces and joint kinematics prediction from sEMG as the exemplar to illustrate the proposed framework. The main contributions can be summarized as: 1) a knowledge embedding data-driven framework is presented, which integrates the physics-based domain knowledge into the data-driven model; 2) the physics-based domain knowledge is regarded as soft constraints to penalise/regularise the loss function of deep neural networks. Physics laws relating to muscle forces and joint kinematics are applied in our case. Without loss of generality, CNN is employed as the deep neural network to implement the proposed framework in this paper. To validate the proposed framework for muscle forces and joint kinematics estimation, a benchmark dataset involving vast walking trials and a self-collected dataset involving wrist motion are employed. Results indicate that the proposed framework with simpler neural network architecture outperforms selected baseline methods, including CNN, multilayer extreme learning machine (ML-ELM), support vector regression (SVR), and extreme learning machine (ELM).

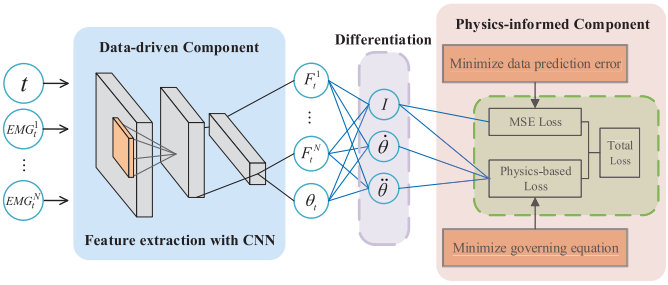

Fig. 1. Main framework of physics-informed deep learning. In this study, inputs of CNN are time steps and EMG signals, while outputs of CNN are muscle forces F_t^n and joint angles θ_t ($n = 1, \ldots, N$, $t = 1, \ldots, T$).

The remaining of this paper is organised as follows: Methodology is detailed in Section II, including the main framework of the proposed physics-informed deep learning method, architecture and training of CNN, and design of loss functions. Material and experimental methods are presented in Section III. Experimental results are reported in Section IV. Finally, discussions are presented in Section V, followed by conclusions in Section VI.

II. Methodology

In this section, we first describe the main framework of the proposed physics-informed deep learning method for musculoskeletal modelling, in the context of muscle forces and joint kinematics prediction from sEMGs. We will elaborate on the main framework, CNN architecture and training, and the designed loss functions below.

A. Physics-Informed Deep Learning Framework

Fig. 1 depicts the main framework of the proposed physics-informed deep learning method for musculoskeletal modelling, in the context of muscle forces and joint kinematics prediction from sEMGs. To be specific, in the data-driven component, CNN is utilised to automatically extract the high-level features and build the relationship between EMG signals and the joint motion/muscle forces, while the physics-informed component entails the underlying physical relationship between the joint motion and muscle forces. In this manner, in the data-driven component, the recorded EMG signals and time steps are first fed into CNN. With the features extracted by CNN, the predicted muscle forces and joint angles could be achieved. Such predictions should also satisfy the physical equation of motion, which is then taken as the soft constraint to penalise/regularise CNN. Finally, a modified total loss function is constructed by integrating the conventional mean square error (MSE) loss and the physics-based loss for the training purpose.

B. Architecture and Training of CNN

To demonstrate the effectiveness of the proposed physics-informed deep learning framework, a very simple

architecture of CNN is employed in this paper. It only consists of one convolutional block, two fully-connected blocks, and one regression block. Specifically, the convolutional block has a convolutional layer, a ReLU layer, a batch normalisation layer, and a dropout layer. It utilises the kernel size of 3, a boundary padding of 3, and a stride of 1 in the convolutional layer. There are 128 kernels in the convolutional layer and a ReLU layer is added subsequently to the convolutional layer. The batch normalisation layer is also considered to mitigate alternation made by the convolutonal layer. Similar to the convolutional block, there are one ReLU layer, one normalisation layer, and one dropout layer in each fully-connected block. The number of hidden nodes is 128. Outputs of the second fully-connected block are then fed into the regression block for the muscle forces and joint kinematics prediction.

In the model training phase, the batch size is set as 1, and CNN is trained by stochastic gradient descent with momentum. Additionally, the maximum iteration is 1200, the initial learning rate is set as 0.01, and the dropout rate is 0.3.

C. Design of Loss Functions

Unlike state-of-the-art methods, the loss function of the proposed framework consists of the MSE loss and the physics-based loss. The MSE loss is to minimise the MSE of the ground truth and prediction, while the physics-based loss preserves the physical constraints during the movements. In this paper, the optimised CNN parameters are achieved based on the total loss below:

$$L_{total} = L_F + L_\theta + L_P \quad (1)$$

$$L_F = MSE(F) \quad (2)$$

$$L_\theta = MSE(\theta) \quad (3)$$

$$L_P = \Phi(F, \theta) \quad (4)$$

where L_F denotes the loss of the muscle force, while L_θ denotes the loss of the joint angle, respectively. L_P represents the loss function imposed by the physics law, which can penalise/regularise CNN for performance enhancement. $\Phi(F, \theta)$ denotes the function of predicted variables.

1) MSE Loss: MSE loss is calculated by

$$\text{MSE}(F) = \frac{1}{T}\sum_{t=1}^{T}\sum_{n=1}^{N}(F_t^n - \hat{F}_t^n)^2 \quad (5)$$

$$\text{MSE}(\theta) = \frac{1}{T}\sum_{t=1}^{T}(\theta_t - \hat{\theta}_t)^2 \quad (6)$$

where F_t^n represents the force of muscle n at time step t, and θ_t denotes the joint angle at time step t, and $\hat{F}_t^n$ and $\hat{\theta}_t$ are their corresponding predicted values from the network, respectively. Additionally, T denotes the total sample number, and N is the total number of muscles at the joint of interest.

2) Physics-Based Loss: Physics-based governing laws, reflecting underlying relationships among the muscle force and kinematics in the human motion, are converted to constraints during the CNN training phase. In this paper, the equation of motion is utilised to design the physics-based loss, which can be mathematically represented as

$$\Phi(F, \theta) = \frac{1}{T}\sum_{t=1}^{T}(M(\theta_t)\ddot{\theta}_t + C(\theta_t, \dot{\theta}_t) + G(\theta_t) - \tau_t)^2 \quad (7)$$

where $M(\theta_t)$, $C(\theta_t, \dot{\theta}_t)$, and $G(\theta_t)$ denote mass matrix, the Centrifugal and Coriolis force, and the gravity, respectively. θ_t denotes the joint angle. τ_t represents the joint torque, which is calculated by the summation of the product of the moment arm and muscle force:

$$\tau_t = \sum_{n=1}^{N} r_n F_t^n \quad (8)$$

where r_n is the moment arm of the muscle n, which is exported from OpenSim.

In this manner, along with the data-driven loss, the physics-based domain knowledge actually plays a regularisation role that enhances the robustness of the created model, and encoding such physical information into a deep neural network could also strengthen the generalisation performance of the proposed framework even when there are only a few training data.

III. Material and Experimental Methods

Two datasets, including one benchmark dataset of walking trials and one self-collected dataset of wrist motions, are utilised to demonstrate the feasibility of the proposed framework.

A. Benchmark Dataset

The walking trails are retrieved from a real-world simulation [32]. This experiment recruited six healthy subjects. The mean age of these subjects was 12.9 ± 3.3 years old, and the mean weight was 51.8 ± 19.2 Kg. Subjects were informed to walking at four different walk speeds, including very slow (0.53 ± 0.04 m/s), slow (0.75 ± 0.10 m/s), free (1.15 ± 0.08 m/s), and fast (1.56 ± 0.21 m/s) speeds.

The data, including GRFs and markers' data, were first band-pass filtered (20 Hz and 450 Hz), fully rectified, and low-pass filtered (6 Hz), respectively. After that, a generic musculoskeletal model with 23 DoFs ('Gait2392') was used [33]. The experimental data were imported to OpenSim to scale the generic musculoskeletal model for each subject [34]. The joint kinematics and joint torque were computed through the inverse kinematic (IK) and inverse dynamic (ID) tools, respectively. The muscle forces were computed using the computed muscle control (CMC) tool to ensure the muscle excitations followed the measured EMGs [35]. Each gait cycle was normalised into 100 frames. We opt to estimate the joint angle and muscle forces at the knee joint during different walking speeds from the EMGs. The *biceps femoris short head* (BFS) and the *rectus femoris* (RF) are chosen as they are the main flexor and extensor of knee joint [36].

Each walking trial is formed to a 100-by-7 matrix consisting of the time step, gait cycle, enveloped EMG signals, and BFS and RF muscle forces. All walking trials are concatenated for

each subject to form a single long matrix for the proposed framework.

B. Self-Collected Dataset

Approved by the MaPS and Engineering Joint Faculty Research Ethics Committee of the University of Leeds (MEEC 18-002), six subjects were recruited to participate in this experiment. All subjects gave signed consent. In the experiment, subjects were informed to maintain a fully straight torso with the 90° abducted shoulder and the 90° flexed elbow joint. The continuous wrist flexion/extension motion was recorded using the VICON motion capture system. The joint motions were computed through the upper limb model using 16 reflective markers (sampled at 250 Hz). Meanwhile, EMG signals were recorded by Avanti Sensors (sampled at 2000 Hz) from the main wrist muscles ($n = 1, 2, \ldots, 5$), including the *flexor carpi radialis* (FCR), the *flexor carpi ulnaris* (FCU), the *extensor carpi radialis longus* (ECRL), the *extensor carpi radialis brevis* (ECRB), and the *extensor carpi ulnaris* (ECU). The electrodes were allocated by palpation and evaluated by performing contraction while looking at the signal before the experiment. Moreover, the EMG signals and motion data were synchronised and resampled at 1000 Hz. Five repetitive trials were performed for each subject, and a three-minute break was given between trials to prevent muscle fatigue.

The measured EMG signals were band-pass filtered (20 Hz and 450 Hz), fully rectified, and low-pass filtered (6 Hz). Then, they were normalised concerning the maximum voluntary contraction recorded before the experiment, resulting in the enveloped EMG signals. The markers' data were used to compute the wrist kinematics via the IK tool according to the upper limb extremity model [37]. Then the joint torque and wrist muscle forces were obtained from the ID and CMC tools to ensure the computed motion was consistent with the measured joint motion.

Each wrist motion trial, consisting of time steps, filtered EMG signals, wrist muscle forces, and wrist joint angles, is formed into a t by 12 matrix.

C. Baseline Methods and Parameters Setting

To verify the effectiveness of the proposed physics-informed deep learning framework, several state-of-the-art methods, including CNN, ML-ELM [38], SVR [39], and ELM [40], are considered as the baseline methods for the comparison. Specifically, CNN has three convolutional blocks, three fully-connected blocks, and one regression block. Stochastic gradient descent with momentum optimiser is employed for CNN training, the batch size is set as 1, the maximum iteration is set as 1200, and the initial learning rate is 0.01. ML-ELM has five hidden layers, and the number of hidden nodes in each hidden layer is determined by the grid search method. ELM is a single hidden layer feedforward neural network, and the Sigmoid function is utilised as the activation function.

D. Evaluation Criteria

To quantify the estimation performance of the proposed framework, root mean square error (RMSE) is first used as the metric. One-way analysis of variance (ANOVA) is also conducted for statistical analysis of the proposed framework and baseline methods. RMSE is the response variable. In specific, RMSE indicates the discrepancies in the amplitude and between the estimated variables and the ground truth, which can be calculated by

$$\text{RMSE} = \sqrt{\frac{1}{T}\sum_{t=1}^{T}(y_t - \hat{y}_t)^2} \tag{9}$$

where y_t and $\hat{y}_t$ indicate the ground truth and the corresponding predicted value, respectively.

Pearson's correlation coefficient (CC) is also employed as another metric, which could be calculated by

$$CC = \frac{\sum_{t=1}^{T}(y_t - \overline{y_t})(\hat{y}_t - \overline{\hat{y}_t})}{\sqrt{\sum_{t=1}^{T}(y_t - \overline{y_t})^2}\sqrt{\sum_{t=1}^{T}(\hat{y}_t - \overline{\hat{y}_t})^2}} \tag{10}$$

where $\overline{y_t}$ and $\overline{\hat{y}_t}$ are the mean of the ground truth and the predicted value, respectively.

IV. Results

In this section, we verify the performance of the proposed framework on knee joint and wrist joint scenarios via comparing with selected baseline methods. Specifically, the training process of the proposed framework is first illustrated. Overall comparisons are then performed to demonstrate the predicted results of the proposed framework and baseline methods, including representative results of the predicted muscle forces and joint angles, and detailed and average predicted results of six healthy subjects. In addition, the intrasession scenario and intersession scenario are also considered to evaluate the robustness and generalisation performance of the proposed framework. Finally, the effects of training dataset sizes, network architectures, and hyperparameters on performance are investigated. The training of the proposed framework and baseline methods is carried out using PyTorch on a workstation with GeForce RTX 2080 Ti graphic cards and 128G RAM.

A. Training Process of the Proposed Framework

To demonstrate the convergence of the proposed framework, we illustrate the convergence process of the total loss of wrist joint case during the training phase in Fig. 2 as the exemplar. For the wrist angle and muscle forces prediction of the wrist joint scenario, the total loss is very low after 200 iterations with small local oscillations as the iteration progresses and actually converges after 600 iterations. We conjecture that the main reason is that we set the batch size as 1 during training CNN. Such batch size could help CNN learn the data distribution better, but it also causes local oscillations. We also would like to point out that for the knee joint case, the same convergence process has also been achieved.

TABLE I
RMSE AND *CC* OF THE PROPOSED FRAMEWORK AND BASELINE METHODS OF KNEE JOINT CASE

Subject	Methods	RF(N)	BFS(N)	Knee Angle(°)	Subject	Methods	RF(N)	BFS(N)	Knee Angle(°)
S1	Ours	18.19/0.92	14.16/0.99	5.69/0.99	S4	Ours	21.51/0.95	15.95/0.99	7.07/0.99
	CNN	20.04/0.89	9.75/0.99	2.17/0.97		CNN	31.66/0.94	16.34/0.99	7.59/0.99
	ML-ELM	25.31/0.86	17.96/0.92	6.01/0.97		ML-ELM	29.74/0.94	19.61/0.99	12.39/0.97
	ELM	35.93/0.82	23.85/0.90	16.82/0.94		ELM	35.80/0.91	26.58/0.93	15.97/0.93
	SVR	33.20/0.81	27.99/0.90	15.33/0.93		SVR	33.29/0.92	23.23/0.93	14.74/0.97
S2	Ours	17.15/0.94	19.83/0.93	4.30/0.99	S5	Ours	13.24/0.97	15.52/0.94	4.71/0.99
	CNN	23.96/0.92	20.95/0.94	3.55/0.98		CNN	15.31/0.95	15.39/0.94	6.97/0.99
	ML-ELM	21.37/0.91	29.62/0.91	9.28/0.94		ML-ELM	19.26/0.95	20.28/0.90	6.05/0.99
	ELM	29.21/0.88	36.25/0.83	17.66/0.91		ELM	30.98/0.90	23.92/0.91	10.22/0.96
	SVR	31.03/0.89	31.53/0.85	14.31/0.90		SVR	25.73/0.89	25.37/0.92	11.36/0.97
S3	Ours	15.51/0.94	13.27/0.92	5.13/0.98	S6	Ours	18.71/0.95	15.47/0.95	5.63/0.98
	CNN	13.20/0.96	17.56/0.92	4.25/0.99		CNN	19.73/0.96	12.55/0.94	7.37/0.98
	ML-ELM	16.77/0.93	21.38/0.93	7.99/0.97		ML-ELM	25.36/0.93	21.34/0.92	8.96/0.97
	ELM	26.35/0.90	26.78/0.90	19.66/0.94		ELM	29.75/0.93	22.53/0.92	12.31/0.94
	SVR	24.60/0.89	22.97/0.90	9.39/0.97		SVR	27.38/0.88	28.70/0.89	15.29/0.95

TABLE II
RMSE AND *CC* OF THE PROPOSED FRAMEWORK AND BASELINE METHODS OF WRIST JOINT CASE

Subject	Methods	FCR(N)	FCU(N)	ECRL(N)	ECRB(N)	ECU(N)	Wrist Angle(°)	Subject	Methods	FCR(N)	FCU(N)	ECRL(N)	ECRB(N)	ECU(N)	Wrist Angle(°)
S1	Ours	3.25/0.99	2.51/0.98	0.79/0.99	2.21/0.99	0.24/0.98	3.76/0.99	S4	Ours	3.91/0.98	2.79/0.99	0.57/0.99	3.26/0.97	0.33/0.99	4.31/0.97
	CNN	2.81/0.99	2.32/0.99	0.90/0.99	1.66/0.99	0.16/0.99	2.30/0.99		CNN	2.89/0.99	3.03/0.99	0.81/0.99	3.36/0.98	0.20/0.99	4.25/0.97
	ML-ELM	5.78/0.97	3.10/0.98	3.51/0.97	3.03/0.96	0.69/0.99	6.98/0.98		ML-ELM	6.33/0.98	4.93/0.97	1.38/0.99	4.90/0.97	0.88/0.99	5.89/0.97
	ELM	10.55/0.93	6.21/0.95	4.77/0.96	3.87/0.96	1.73/0.98	12.33/0.93		ELM	8.27/0.96	7.38/0.95	3.55/0.97	5.73/0.95	1.03/0.99	10.55/0.94
	SVR	6.34/0.97	7.92/0.95	5.32/0.93	5.10/0.96	0.99/0.97	8.57/0.94		SVR	9.36/0.95	7.62/0.95	4.30/0.97	5.46/0.96	1.52/0.99	9.33/0.93
S2	Ours	4.21/0.99	2.63/0.99	0.71/0.99	3.25/0.98	0.58/0.99	2.77/0.99	S5	Ours	2.53/0.98	3.52/0.99	1.21/0.98	2.91/0.99	0.65/0.99	3.45/0.99
	CNN	4.29/0.99	3.96/0.99	0.99/0.99	2.98/0.99	0.37/0.99	2.59/0.99		CNN	2.31/0.98	3.49/0.98	1.79/0.98	2.03/0.99	0.71/0.99	2.99/0.99
	ML-ELM	7.30/0.98	3.27/0.98	2.38/0.97	3.57/0.99	0.95/0.99	4.30/0.96		ML-ELM	6.38/0.94	4.33/0.97	3.59/0.98	3.87/0.98	1.01/0.99	7.56/0.96
	ELM	11.25/0.94	7.99/0.98	2.95/0.97	7.98/0.98	2.09/0.99	7.62/0.96		ELM	9.22/0.94	6.27/0.93	8.26/0.97	5.66/0.98	2.89/0.99	10.30/0.92
	SVR	11.03/0.94	9.28/0.98	4.17/0.94	6.22/0.98	1.28/0.99	6.53/0.97		SVR	8.89/0.93	9.35/0.92	6.30/0.96	7.27/0.97	2.50/0.99	11.28/0.93
S3	Ours	5.18/0.98	3.77/0.98	0.97/0.99	4.96/0.97	0.41/0.99	4.30/0.97	S6	Ours	6.20/0.98	4.17/0.98	0.91/0.99	3.89/0.99	0.33/0.99	5.81/0.97
	CNN	3.99/0.99	4.59/0.98	1.23/0.99	6.83/0.98	0.47/0.99	3.94/0.98		CNN	4.27/0.98	5.35/0.96	0.99/0.99	5.36/0.97	0.56/0.99	6.21/0.98
	ML-ELM	7.89/0.96	4.51/0.97	4.37/0.98	7.31/0.96	0.92/0.99	6.88/0.99		ML-ELM	6.34/0.97	7.95/0.96	2.57/0.99	7.90/0.95	0.79/0.99	8.30/0.96
	ELM	12.33/0.93	8.26/0.95	6.25/0.95	7.15/0.96	2.02/0.99	9.37/0.94		ELM	10.28/0.94	9.21/0.96	4.43/0.98	5.21/0.95	2.37/0.98	10.22/0.96
	SVR	11.76/0.94	7.93/0.95	7.01/0.95	8.89/0.94	1.78/0.98	7.55/0.93		SVR	10.04/0.94	8.89/0.94	4.21/0.98	5.12/0.96	2.17/0.99	8.95/0.97

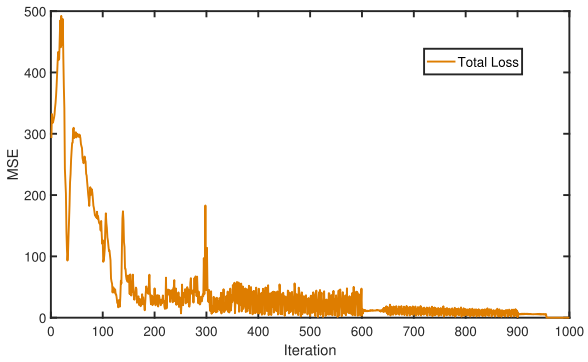

Fig. 2. Illustration of the total loss of wrist joint case.

B. Overall Comparisons

The overall comparisons between the proposed framework and baseline methods are first performed. Fig. 3 and Fig. 4 depict the representative results of the proposed framework for the knee joint case and the wrist joint case, including the knee flexion angle, muscle force of RF, muscle force of BFS, wrist flexion angle, muscle force of FCR, muscle force of FCU, muscle force of ECRL, muscle force of ECRB, and muscle force of ECU, respectively. As we can see from Fig. 3 and Fig. 4, the predicted values of muscle forces and joint angles could fit the ground truths well, indicating the great dynamic tracking capability of the proposed framework.

To quantitatively evaluate the performance of the proposed framework, detailed comparisons of all the subjects between the proposed framework and baseline methods are presented in Table I and Table II. It should be noted that we use the data with the same walking speed to train and test the proposed framework and baseline methods in the knee joint case. According to Table I and Table II, the proposed framework could achieve smaller RMSEs and higher *CC*s in most cases, which further verifies the robustness of the proposed framework. To be specific, deep learning-based methods, including the proposed framework, CNN and ML-ELM, achieve better predicted performance than machine learning-based methods, including SVR and ELM. Because these deep learning-based methods could automatically extract high-level features from the collected data. Among deep learning-based methods, the proposed framework achieves the best predicted performance, because the embedded physics law could penalise/regularise CNN utilised in the proposed framework, its performance is not only dependent on the conventional MSE loss, but also can be enhanced by the physics-based loss.

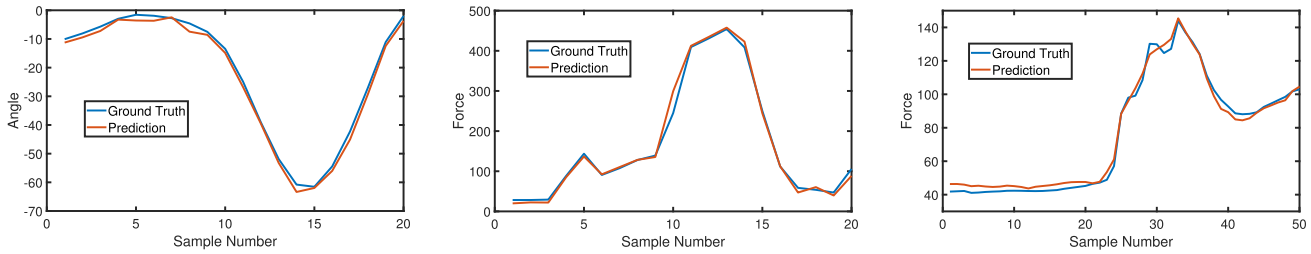

(a) Predicted results of knee angle (b) Predicted results of BFS (c) Predicted results of RF

Fig. 3. Representative results of the knee joint case through the proposed physics-informed data-driven model. The predicted outputs of the knee joint case include the knee angle, BFS muscle force, and RF muscle force.

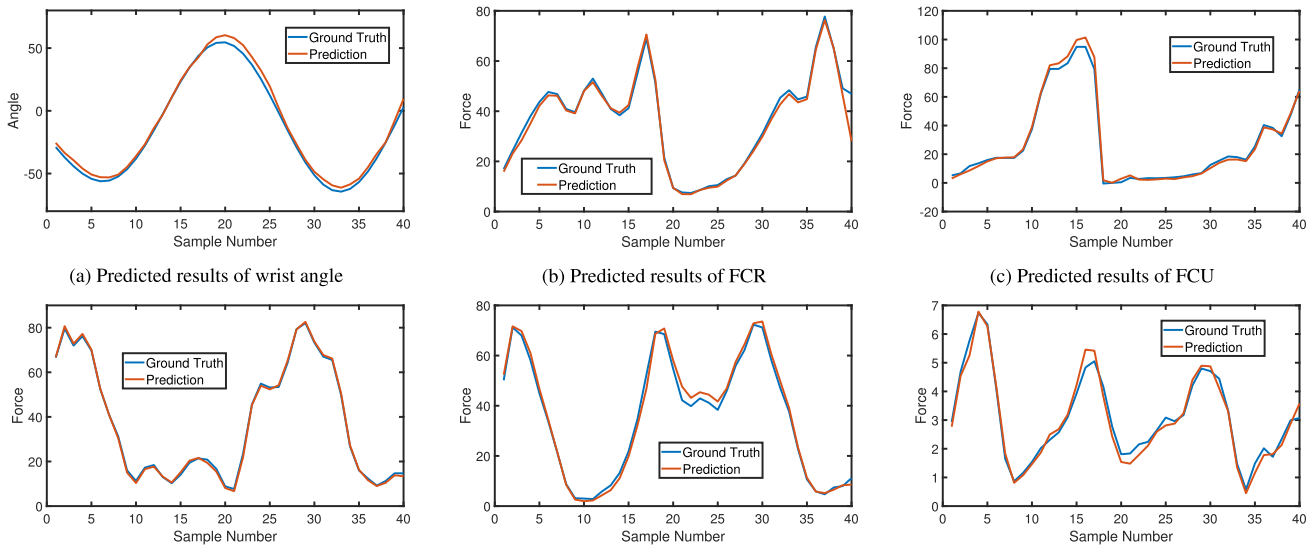

(a) Predicted results of wrist angle (b) Predicted results of FCR (c) Predicted results of FCU

(d) Predicted results of ECRL (e) Predicted results of ECRB (f) Predicted results of ECU

Fig. 4. Representative results of the wrist joint case through the knowledge embedding data-driven model. The predicted outputs of the wrist joint case include the wrist angle, FCR muscle force, FCU muscle force, ECRL muscle force, ECRB muscle force, and ECU muscle force.

Aside from the overall comparisons of the five approaches, we further carried out a pairwise analysis between the proposed framework and each comparison method on the two datasets. A *post-hoc* analysis using Tukey's Honest Significant Difference test is applied. The significance level is set at $p < 0.05$. Fig. 5 illustrates the average RMSEs of the knee and wrist joints of the proposed framework and baseline methods across all the subjects. As observed from Fig. 5, the proposed framework achieves satisfactory performance with lower standard deviations, and its predicted results are with smaller fluctuations. Moreover, with simple neural network architecture, the proposed framework could achieve comparable performance compared with pure CNN, which has a more complex network architecture, by embedding the underlying physical interactions between predicted variables into the data-driven model. This motivates us to employ more constraints to deeply integrate the knowledge of the musculoskeletal modelling into the deep neural network to enhance the performance in the future work.

C. Evaluation of Intrasession Scenario

The intrasession scenario is also considered to validate the robustness of the proposed framework. For each subject, the data with different walking speeds are fused into a whole dataset, where 80% for training and the rest 20% for testing. Fig. 6 depicts the corresponding experimental results, in which the proposed framework outperforms most baseline methods. According to Fig. 6, the proposed framework is not affected by the walking speeds, but the predicted results of some baseline methods are degraded. For instance, the predicted performance of SVR for muscle force of RF prediction illustrated in Fig. 5(a) is better than that of ELM, but its predicted performance becomes worse in the intrasession scenario due to the effects of different walking speeds.

D. Evaluation of Intersession Scenario

To investigate the performance of the proposed framework on the unseen data, we evaluate the proposed framework in the intersession scenario. The training dataset consists of the data from five subjects, and the 6th subject's data construct the testing dataset. Table III demonstrates the detailed results, we can find that the proposed framework still can achieve satisfactory performance, which indicates its great generalisation.

E. Effects of Training Dataset Sizes

To evaluate the effects of the training dataset sizes on the prediction performance, we illustrate the normalised RMSEs

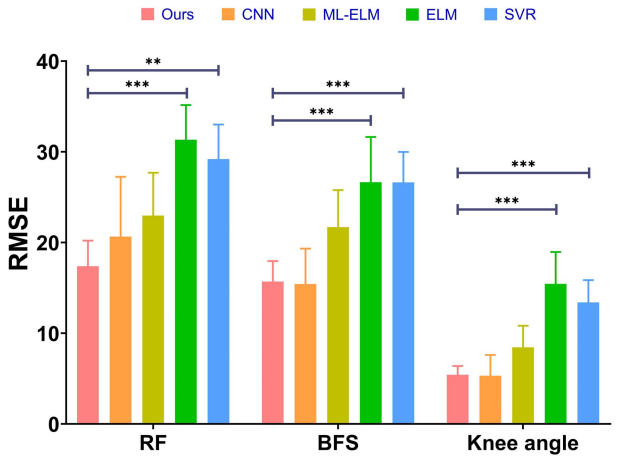

(a) Average RMSEs of knee joint case

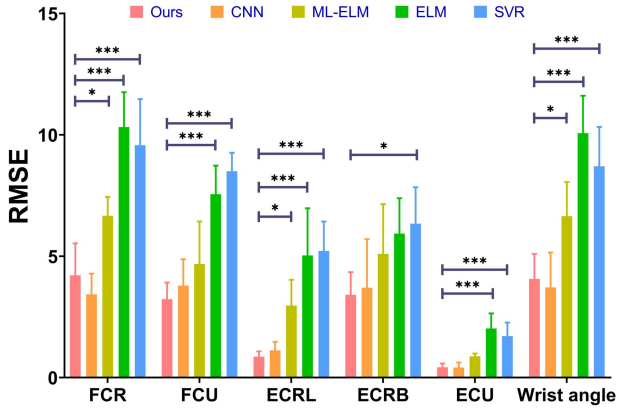

(b) Average RMSEs of wrist joint case

Fig. 5. Average RMSEs across all the subjects in (a) knee joint and (b) wrist joint scenarios, respectively. The proposed framework achieves comparable RMSEs with simpler CNN architecture compared with pure CNN. Compared with ML-ELM, ELM and SVR, the proposed framework achieves better and more stable prediction performance. The significance level is set as 0.05 ($^{***}p < 0.001, ^{**}p < 0.01$, *and* $^{*}p < 0.05$).

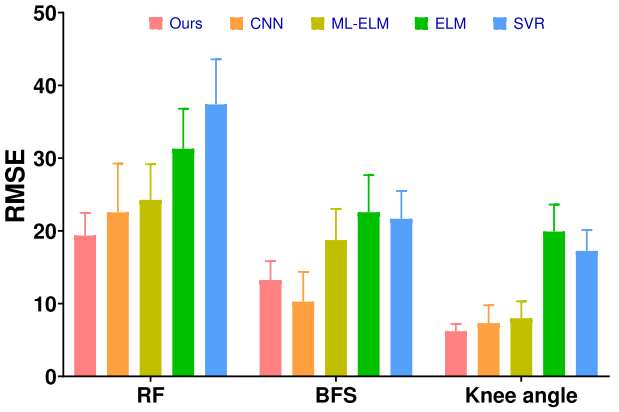

Fig. 6. Comparison results of intrasession scenario.

of the wrist joint case of the proposed framework and baseline methods under different training dataset sizes in Fig. 7. The normalised RMSEs of the proposed framework and baseline methods become low with the increase of training dataset

TABLE III
COMPARISONS OF THE PROPOSED FRAMEWORK AND BASELINE METHODS IN INTERSESSION SCENARIO (RMSE)

Variables	Ours	CNN	ML-ELM	ELM	SVR
RF	23.77	25.15	29.91	38.29	37.03
BFS	22.30	23.98	27.02	30.99	31.21
Angle	7.82	7.76	10.65	14.51	13.29

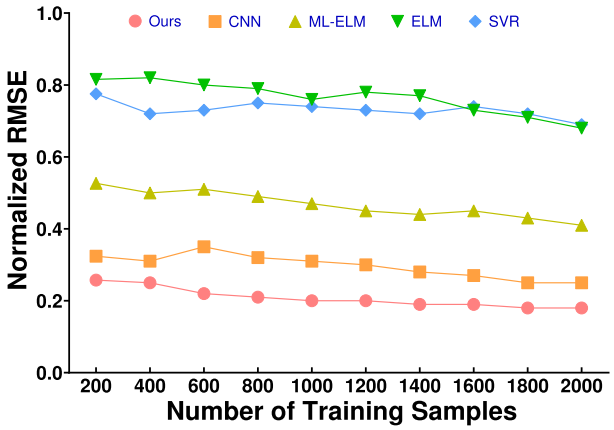

Fig. 7. Effects of the training dataset sizes on prediction performance of the wrist joint case. The proposed framework achieves a faster convergence speed with simpler network architecture.

sizes, but the proposed framework, on the other side, could achieve lower normalised RMSEs with fewer training samples. Experimental results indicate the proposed framework is less sensitive to the training dataset size. Embedded physics-based domain knowledge as the penalisation/regularisation term in the loss function of CNN yields faster convergence speed and reduces requirements in training data for a given performance.

F. Effects of Network Architectures

To further evaluate the proposed framework, we illustrate the comparison results of the wrist joint case of the proposed framework and CNN under the same network architecture, i.e., both CNN in the proposed framework and pure CNN have three convolutional blocks, three fully-connected blocks, and one regression block, in Fig. 8. According to Fig. 8, the proposed framework could achieve better prediction performance than CNN, further indicating the effectiveness of the physics law embedded in the proposed framework.

To further investigate the effects of network architectures on the performance of the proposed framework, we implement the proposed framework with various network architectures, including one convolutional block (named PINN-1), two convolutional blocks (named PINN-2), three convolutional blocks (named PINN-3), four convolutional blocks (named PINN-4), and five convolutional blocks (named PINN-5), for the knee joint case. Table IV lists the detailed comparison results, we can find that the proposed framework could achieve the best performance with three convolutional blocks, and its accuracy becomes better with the increase of the number of convolutional blocks, this is because more representative

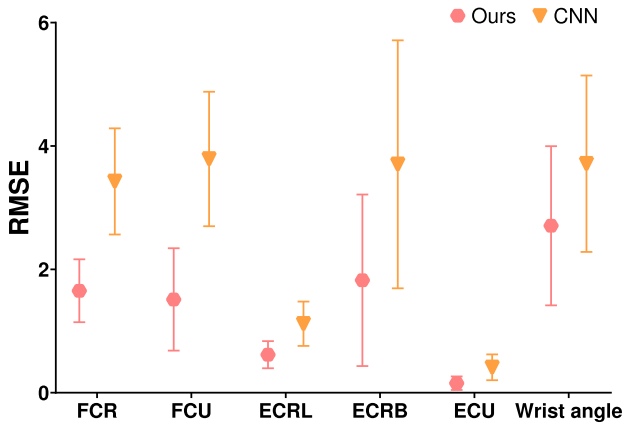

Fig. 8. Comparison results between the proposed framework and CNN under the same network architecture. The proposed framework achieves better predicted results without considering the effects of network architecture.

TABLE IV
COMPARISONS OF THE PROPOSED FRAMEWORK UNDER VARIOUS NETWORK ARCHITECTURES (RMSE)

Variables	PINN-1	PINN-2	PINN-3	PINN-4	PINN-5
RF	19.32	15.51	13.39	15.01	21.89
BFS	15.27	8.82	7.93	8.95	12.72
Angle	5.73	2.36	2.02	2.87	7.56

features can be extracted with appropriate number of convolutional blocks (such as PINN-3), but the proposed framework may be over-fitting if we continue to increase the number of convolutional blocks (such as PINN-5).

G. Effects of Hyperparameters

We also investigate the effects of hyperparameters, including learning rate, types of activation functions, and batch size, on the performance of the proposed framework using the wrist joint case, and the detailed results are shown in Table V, Table VI, and Table VII. Specifically, we consider three different learning rates, i.e., 0.01, 0.001 and 0.0001, and the maximum iterations is set as 400. According to Table V, we can find that the proposed framework achieves better performance with smaller learning rate. Observed from Table VI, the proposed framework with ReLU and Leaky ReLU could achieve comparable performance, but better than the one using Sigmoid as the activation function. In Table VII, the performance of the proposed framework achieves better performance with the increase of the batch size, this is because the larger batch size can reduce the local oscillations during the training process and guarantee the performance of the deep neural network.

V. DISCUSSIONS AND FUTURE DIRECTIONS

In this section, we first discuss the flexibility of the proposed framework, and essential advantages of physics-informed deep learning in musculoskeletal modelling are then presented, respectively. Finally, limitations of this work and future directions are considered.

TABLE V
COMPARISONS OF THE PROPOSED FRAMEWORK UNDER VARIOUS LEARNING RATES (RMSE)

Learning Rates	FCR	FCU	ECRL	ECRB	ECU	Angle
0.01	15.25	12.51	10.79	12.21	3.24	10.06
0.001	9.03	11.19	8.68	9.09	1.22	8.29
0.0001	6.69	9.76	8.52	8.67	1.92	6.51

TABLE VI
COMPARISONS OF THE PROPOSED FRAMEWORK UNDER DIFFERENT TYPES OF ACTIVATION FUNCTIONS (RMSE)

Activation Functions	FCR	FCU	ECRL	ECRB	ECU	Angle
Sigmoid	5.37	4.50	1.21	3.63	0.77	5.29
ReLU	3.25	2.51	0.79	2.21	0.24	3.76
Leaky ReLU	3.22	2.56	0.73	2.25	0.39	3.97

TABLE VII
COMPARISONS OF THE PROPOSED FRAMEWORK UNDER VARIOUS BATCH SIZES (RMSE)

Activation Functions	FCR	FCU	ECRL	ECRB	ECU	Angle
1	3.25	2.51	0.79	2.21	0.24	3.76
32	3.17	2.32	0.65	2.01	0.20	3.55
64	3.19	2.29	0.66	1.97	0.21	3.37

A. Flexibility of the Proposed Framework

The proposed framework is a generic paradigm for incorporating mechanistic musculoskeletal constraints. In this paper, we utilise a specific case, i.e., joint angle and muscle force prediction, as the exemplar to demonstrate the feasibility of this approach. Here, a CNN with simpler architecture is used as the data-driven modelling technique to extract feature maps from kinematics to muscle forces and EMG to motion, respectively. However, we can also change the deep network's inputs and outputs to satisfy different application scenarios, i.e., use EMG/kinematics to predict muscle force and activation for robot-assisted rehabilitation, use kinematics data to predict muscle force and activation for musculoskeletal diseases diagnosis, and use EMG to predict kinematics for prosthetic control.

In addition, all the components in the proposed framework can be withdrawn or adjusted, and new components could be incorporated into this framework depending on application demands. For example, in addition to CNN, the deep neural network in the data-driven component can be replaced by CNN+LSTM when we want to extract spatial and temporal representations from kinematic measurements [41], or generative adversarial network (GAN) when domain-independent features are required [42]. Moreover, few-shot learning should be considered when only a few training data are available [43], or federated learning is preferred when addressing data privacy issues [44].

For the physics-based component, we only used equation of motion in this paper. However, the physics law can also be further expanded. For instance, we can also incorporate the

Hill muscle model into the proposed framework, the predicted force should be equal to the Hill muscle model prediction, which can be used as the second physics law in the network. In addition, more soft constraints can also be imposed, i.e., our body geometrical constraint, and multiple joints coordination, etc., to enhance the deep neural network performance.

Although we only consider the wrist joint and knee joint cases as the exemplar, and we would envisage that the proposed framework would also be applicable to more complex musculoskeletal models, such as full lower body model for walking. The only difference would be to increase the network input/output dimensions, and incorporate more physics laws in the model.

B. Understanding Physics-Informed Data-Driven Methods for Musculoskeletal Modeling

Machine/deep learning methods have been utilised for musculoskeletal modelling, because they are conceptually intuitive simple and fast to implement [23], [45], [46], [47]. However, while they may fit kinematic measurements very well in the training stage, their predictions may not satisfy the physics associated with musculoskeletal biomechanics. This may lead to poor robustness and generalisation. In addition, data-driven methods provide limited interpretability from kinematic measurements. In contrast, physics-informed deep learning seamlessly integrates physics-based domain knowledge into deep learning and hence informative constraints for performance enhancement [48], [49], [50]. In physics-informed deep learning, we incorporate domain knowledge that from kinematic measurements and the physical understanding of the neuromusculoskeletal coupling. In this manner, deep learning methods are interpretable, reflecting physical or physiological mechanisms, and more robust and generalise better even with limited training data.

C. Limitations and Future Directions

In this study, we only consider the wrist joint and knee joint cases as the exemplar to implement the proposed framework and verify its feasibility. We will further investigate properties of the physics-informed deep learning framework in musculoskeletal modelling. For example, we are planning to explore the effects of weights imposing on the two loss components on the performance. We will also change the inputs and outputs of the data-driven component of the proposed framework to satisfy different application scenarios. Moreover, the reliability and accuracy of the proposed framework will also be evaluated via more complicated movement involving multiple joints movements.

VI. Conclusion

This paper develops a knowledge embedding data-driven framework, which seamlessly integrates the physics-based domain knowledge into the data-driven model, for musculoskeletal modelling. Specifically, the physics-based domain knowledge is utilised as soft constraints to penalise/regularise the deep neural network to enhance the robustness and generalisation performance, and computational demands in model building are significantly reduced. Comprehensive experiments on two groups of data for muscle forces and joint angles prediction indicate the feasibility of the proposed framework. We envision that the proposed framework is a general methodology for both muscle forces and joint angles prediction, and other applications in the musculoskeletal modelling field, which may reduce the gaps between laboratory prototypes and clinical applications.

References

[1] A. Rajagopal, C. L. Dembia, M. S. DeMers, D. D. Delp, J. L. Hicks, and S. L. Delp, "Full-body musculoskeletal model for muscle-driven simulation of human gait," *IEEE Trans. Biomed. Eng.*, vol. 63, no. 10, pp. 2068–2079, Oct. 2016.

[2] J. Berning, G. E. Francisco, S.-H. Chang, B. J. Fregly, and M. K. O'Malley, "Myoelectric control and neuromusculoskeletal modeling: Complementary technologies for rehabilitation robotics," *Curr. Opin. Biomed. Eng.*, vol. 19, pp. 1–7, Sep. 2021.

[3] R. Zaman, Y. Xiang, R. Rakshit, and J. Yang, "Hybrid predictive model for lifting by integrating skeletal motion prediction with an OpenSim musculoskeletal model," *IEEE Trans. Biomed. Eng.*, vol. 69, no. 3, pp. 1111–1122, Mar. 2022.

[4] S. A. McErlain-Naylor, M. A. King, and P. J. Felton, "A review of forward-dynamics simulation models for predicting optimal technique in maximal effort sporting movements," *Appl. Sci.*, vol. 11, no. 4, pp. 1450–1469, 2021.

[5] T. Akbas, R. R. Neptune, and J. Sulzer, "Neuromusculoskeletal simulation reveals abnormal rectus femoris-gluteus medius coupling in post-stroke gait," *Frontiers Neurol.*, vol. 10, pp. 1–10, Apr. 2019.

[6] L. S. Persad, B. I. Binder-Markey, A. Y. Shin, K. R. Kaufman, and R. L. Lieber, "*In vivo* human gracilis whole-muscle passive stress–sarcomere strain relationship," *J. Experim. Biol.*, vol. 224, no. 17, pp. 1–9, Sep. 2021.

[7] Q. Zhang, W. H. Clark, J. R. Franz, and N. Sharma, "Personalized fusion of ultrasound and electromyography-derived neuromuscular features increases prediction accuracy of ankle moment during plantarflexion," *Biomed. Signal Process. Control*, vol. 71, Jan. 2022, Art. no. 103100.

[8] M. K. Jung et al., "Intramuscular EMG-driven musculoskeletal modelling: Towards implanted muscle interfacing in spinal cord injury patients," *IEEE Trans. Biomed. Eng.*, vol. 69, no. 1, pp. 63–74, Jan. 2022.

[9] Y. Zhao et al., "Computational efficient personalised EMG-driven musculoskeletal model of wrist joint," *IEEE Trans. Instrum. Meas.*, early access, Nov. 28, 2022, doi: 10.1109/TIM.2022.3225023.

[10] K. J. Bennett et al., "EMG-informed neuromusculoskeletal models accurately predict knee loading measured using instrumented implants," *IEEE Trans. Biomed. Eng.*, vol. 69, no. 7, pp. 2268–2275, Jul. 2022.

[11] V. Chambers and P. Artemiadis, "A model-based analysis of supraspinal mechanisms of inter-leg coordination in human gait: Toward model-informed robot-assisted rehabilitation," *IEEE Trans. Neural Syst. Rehabil. Eng.*, vol. 29, pp. 740–749, 2021.

[12] S. Park, G. E. Caldwell, and B. R. Umberger, "A direct collocation framework for optimal control simulation of pedaling using OpenSim," *PLoS ONE*, vol. 17, no. 2, pp. 1–17, 2022.

[13] J. Zhao, Y. Yu, X. Wang, S. Ma, X. Sheng, and X. Zhu, "A musculoskeletal model driven by muscle synergy-derived excitations for hand and wrist movements," *J. Neural Eng.*, vol. 19, no. 1, Feb. 2022, Art. no. 016027.

[14] Y. Zhao, Z. Zhang, Z. Li, Z. Yang, A. A. Dehghani-Sanij, and S. Xie, "An EMG-driven musculoskeletal model for estimating continuous wrist motion," *IEEE Trans. Neural Syst. Rehabil. Eng.*, vol. 28, no. 12, pp. 3113–3120, Dec. 2020.

[15] M. Sartori, D. Farina, and D. G. Lloyd, "Hybrid neuromusculoskeletal modeling to best track joint moments using a balance between muscle excitations derived from electromyograms and optimization," *J. Biomechanics*, vol. 47, no. 15, pp. 3613–3621, Nov. 2014.

[16] C. Pizzolato, M. Reggiani, D. J. Saxby, E. Ceseracciu, L. Modenese, and D. G. Lloyd, "Biofeedback for gait retraining based on real-time estimation of tibiofemoral joint contact forces," *IEEE Trans. Neural Syst. Rehabil. Eng.*, vol. 25, no. 9, pp. 1612–1621, Sep. 2017.

[17] G. Hajian and E. Morin, "Deep multi-scale fusion of convolutional neural networks for EMG-based movement estimation," *IEEE Trans. Neural Syst. Rehabil. Eng.*, vol. 30, pp. 486–495, 2022.

[18] C. Wu, H. Zeng, A. Song, and B. Xu, "Grip force and 3D push-pull force estimation based on sEMG and GRNN," *Frontiers Neurosci.*, vol. 11, pp. 1–15, Jun. 2017.
[19] C. G. McDonald, J. L. Sullivan, T. A. Dennis, and M. K. O'Malley, "A myoelectric control interface for upper-limb robotic rehabilitation following spinal cord injury," *IEEE Trans. Neural Syst. Rehabil. Eng.*, vol. 28, no. 4, pp. 978–987, Apr. 2020.
[20] T. Bao, S. Q. Xie, P. Yang, P. Zhou, and Z.-Q. Zhang, "Toward robust, adaptiveand reliable upper-limb motion estimation using machine learning and deep learning—A survey in myoelectric control," *IEEE J. Biomed. Health Informat.*, vol. 26, no. 8, pp. 3822–3835, Aug. 2022.
[21] R. Hu, X. Chen, H. Zhang, X. Zhang, and X. Chen, "A novel myoelectric control scheme supporting synchronous gesture recognition and muscle force estimation," *IEEE Trans. Neural Syst. Rehabil. Eng.*, vol. 30, pp. 1127–1137, 2022.
[22] Y. Geng et al., "A CNN-attention network for continuous estimation of finger kinematics from surface electromyography," *IEEE Robot. Autom. Lett.*, vol. 7, no. 3, pp. 6297–6304, Jul. 2022.
[23] L. Rane, Z. Ding, A. H. McGregor, and A. M. J. Bull, "Deep learning for musculoskeletal force prediction," *Ann. Biomed. Eng.*, vol. 47, no. 3, pp. 778–789, Mar. 2019.
[24] T. Bao, S. A. R. Zaidi, S. Xie, P. Yang, and Z.-Q. Zhang, "Inter-subject domain adaptation for CNN-based wrist kinematics estimation using sEMG," *IEEE Trans. Neural Syst. Rehabil. Eng.*, vol. 29, pp. 1068–1078, 2021.
[25] Y. Huang et al., "Real-time intended knee joint motion prediction by deep-recurrent neural networks," *IEEE Sensors J.*, vol. 19, no. 23, pp. 11503–11509, Aug. 2019.
[26] A. Ameri, M. A. Akhaee, E. Scheme, and K. Englehart, "Real-time, simultaneous myoelectric control using a convolutional neural network," *PLoS ONE*, vol. 13, no. 9, pp. 1–13, 2018.
[27] H. Su, W. Qi, Z. Li, Z. Chen, G. Ferrigno, and E. De Momi, "Deep neural network approach in EMG-based force estimation for human–robot interaction," *IEEE Trans. Artif. Intell.*, vol. 2, no. 5, pp. 404–412, Oct. 2021.
[28] W. S. Burton, C. A. Myers, and P. J. Rullkoetter, "Machine learning for rapid estimation of lower extremity muscle and joint loading during activities of daily living," *J. Biomechanics*, vol. 123, Jun. 2021, Art. no. 110439.
[29] W. R. Johnson, J. Alderson, D. Lloyd, and A. Mian, "Predicting athlete ground reaction forces and moments from spatio-temporal driven CNN models," *IEEE Trans. Biomed. Eng.*, vol. 66, no. 3, pp. 689–694, Mar. 2019.
[30] G. E. Karniadakis et al., "Physics-informed machine learning," *Nat. Rev. Phys.*, vol. 3, no. 6, pp. 422–440, 2021.
[31] M. Raissi, P. Perdikaris, and G. E. Karniadakis, "Physics-informed neural networks: A deep learning framework for solving forward and inverse problems involving nonlinear partial differential equations," *J. Comput. Phys.*, vol. 378, pp. 686–707, Feb. 2019.
[32] M. Q. Liu, F. C. Anderson, M. H. Schwartz, and S. L. Delp, "Muscle contributions to support and progression over a range of walking speeds," *J. Biomech.*, vol. 41, no. 15, pp. 3243–3252, Nov. 2008.
[33] S. L. Delp, J. P. Loan, M. G. Hoy, F. E. Zajac, E. L. Topp, and J. M. Rosen, "An interactive graphics-based model of the lower extremity to study orthopaedic surgical procedures," *IEEE Trans. Biomed. Eng.*, vol. 37, no. 8, pp. 757–767, Aug. 1990.
[34] A. Seth et al., "OpenSim: Simulating musculoskeletal dynamics and neuromuscular control to study human and animal movement," *PLoS Comput. Biol.*, vol. 14, no. 7, pp. 1–20, Jul. 2018.
[35] D. G. Thelen, F. C. Anderson, and S. L. Delp, "Generating dynamic simulations of movement using computed muscle control," *J. Biomech.*, vol. 36, no. 3, pp. 321–328, 2003.
[36] Y. Ma, S. Xie, and Y. Zhang, "A patient-specific EMG-driven neuromuscular model for the potential use of human-inspired gait rehabilitation robots," *Comput. Biol. Med.*, vol. 70, pp. 88–98, Mar. 2016.
[37] D. C. McFarland, E. M. McCain, M. N. Poppo, and K. R. Saul, "Spatial dependency of glenohumeral joint stability during dynamic unimanual and bimanual pushing and pulling," *J. Biomech. Eng.*, vol. 141, no. 5, May 2019, Art. no. 051006.
[38] J. Zhang, Y. Li, W. Xiao, and Z. Zhang, "Non-iterative and fast deep learning: Multilayer extreme learning machines," *J. Franklin Inst.*, vol. 357, no. 13, pp. 8925–8955, 2020.
[39] H. Zhang, Y. Guo, and D. Zanotto, "Accurate ambulatory gait analysis in walking and running using machine learning models," *IEEE Trans. Neural Syst. Rehabil. Eng.*, vol. 28, no. 1, pp. 191–202, Dec. 2020.
[40] J. Zhang, W. Xiao, Y. Li, and S. Zhang, "Residual compensation extreme learning machine for regression," *Neurocomputing*, vol. 311, pp. 126–136, Oct. 2018.
[41] T. Bao, S. A. R. Zaidi, S. Xie, P. Yang, and Z.-Q. Zhang, "A CNN-LSTM hybrid model for wrist kinematics estimation using surface electromyography," *IEEE Trans. Instrum. Meas.*, vol. 70, pp. 1–9, 2020.
[42] A. Creswell, T. White, V. Dumoulin, K. Arulkumaran, B. Sengupta, and A. A. Bharath, "Generative adversarial networks: An overview," *IEEE Signal Process.*, vol. 35, no. 1, pp. 53–65, Jan. 2018.
[43] Y. Wang, Q. Yao, J. T. Kwok, and L. M. Ni, "Generalizing from a few examples: A survey on few-shot learning," *ACM Comput. Surv.*, vol. 53, no. 3, pp. 1–34, 2020.
[44] T. Li, A. K. Sahu, A. Talwalkar, and V. Smith, "Federated learning: Challenges, methods, and future directions," *IEEE Signal Process. Mag.*, vol. 37, no. 3, pp. 50–60, May 2020.
[45] J. Zhang, Y. Li, and W. Xiao, "Adaptive online sequential extreme learning machine for dynamic modeling," *Soft Comput.*, vol. 25, no. 3, pp. 2177–2189, Feb. 2021.
[46] T. T. Dao, "From deep learning to transfer learning for the prediction of skeletal muscle forces," *Med. Biol. Eng. Comput.*, vol. 57, no. 5, pp. 1049–1058, 2019.
[47] D. J. Saxby et al., "Machine learning methods to support personalized neuromusculoskeletal modelling," *Biomech. Model Mechanobiol.*, vol. 19, no. 4, pp. 1169–1185, 2020.
[48] S. Wang, X. Yu, and P. Perdikaris, "When and why PINNs fail to train: A neural tangent kernel perspective," *J. Comput. Phys.*, vol. 449, pp. 1–28, Jan. 2022.
[49] A. D. Jagtap, E. Kharazmi, and G. E. Karniadakis, "Conservative physics-informed neural networks on discrete domains for conservation laws: Applications to forward and inverse problems," *Comput. Methods Appl. Mech. Eng.*, vol. 365, pp. 1–27, Jun. 2020.
[50] L. Von Rueden et al., "Informed machine learning—A taxonomy and survey of integrating knowledge into learning systems," *IEEE Trans. Knowl. Data Eng.*, early access, May 12, 2021, doi: 10.1109/TKDE.2021.3079836.